Published in final edited form as:
Ann Biomed Eng. 2014 August ; 42(8): 1658–1667. doi:10.1007/s10439-014-1017-5.

An in vivo Rat Model of Artery Buckling for Studying Wall Remodeling

Jinzhou Zhang[1,2,*], **Qin Liu**[1,*], and **Hai-Chao Han**[1]

[1]Department of Mechanical Engineering, University of Texas at San Antonio

[2]Department of Cardiovascular Surgery, Xijing Hospital, Fourth Military Medical University, China

Abstract

Theoretical modeling and *in vitro* experiments have demonstrated that arterial buckling is a possible mechanism for the development of artery tortuosity. However, there has been no report of whether artery buckling develops into tortuosity, partially due to the lack of *in vivo* models for long-term studies. The objective of this study was to establish an *in vivo* buckling model in rat carotid arteries for studying arterial wall remodeling after buckling. Rat left carotid arteries were transplanted to the right carotid arteries to generate buckling under in vivo pressure and were maintained for 1 week to examine wall remodeling and adaptation. Our results showed that a significant buckling was achieved in the carotid arterial grafts with altered wall stress. Cell proliferation and matrix metalloprotinease-2 (MMP-2) expression in the buckled arteries increased significantly compared with the controls. The tortuosity level of the grafts also slightly increased 1 week post-surgery, while there was no change in vessel dimensions, blood pressure, and blood flow velocity. The artery buckling model provides a useful tool for further study of the adaptation of arteries into tortuous shapes.

Keywords

artery remodeling; adaptation; buckling; tortuosity; cell proliferation; MMP-2/-9; animal model

Introduction

Tortuosity is often seen in internal carotid arteries, iliac arteries, coronary arteries, retinal arteries, and conjunctival arteries.[3, 6, 17, 25, 31, 33] Clinical studies have demonstrated that artery tortuosity is associated with hypertensive blood pressure, aging, atherosclerosis, genetic defects, and other diseases.[1, 2, 6, 17, 20] However, the underlying biomechanical mechanisms that lead to artery tortuosity remain unclear.

Recently, we have proposed that mechanical instability, i.e. artery buckling, could be a possible mechanism for the initiation of tortuous arteries.[15, 17] Our theoretical analysis and

Address Correspondence to: Dr. Hai-Chao Han, Department of Mechanical Engineering, The University of Texas at San Antonio, San Antonio, TX 78249, Tel: (210) 458-4952, Fax: (210) 458-6504, haichao.han@utsa.edu.

*Equally contributed to this work

Conflict of interest

The authors have no conflict of interest.

in vitro experimental studies have demonstrated that arteries would lose mechanical stability and buckle into tortuous shapes due to hypertensive pressure, reduced axial tension, or reduced wall stiffness.[13, 15, 28] Computational simulation also demonstrated that axial or radial growth could lead to the loss of stability and buckling in collateral arterioles.[29] The tortuous path resulting from artery buckling changes the flow and wall stress in the arteries.[17] It is well known that changes in mechanical stress (either shear stress on the lumen or tensile stress in the wall) would lead to arterial wall remodeling.[7, 22, 24] Therefore, it is important to understand how buckled arteries remodel over time and whether they will develop into permanently tortuous vessels. Animal models have been used as an effective approach for studying the long-term arterial wall remodeling; however, there has been no report of animal model of artery buckling.

Therefore, the **objective** of this study was to develop an *in vivo* artery buckling model suitable for investigating wall remodeling. Using a left-to-right carotid artery grafting technique, we developed an artery buckling model in rats and investigated the early changes in the tortuosity index and wall remodeling in these buckled arteries.

Materials and Methods

Male Sprague Dawley rats (8–10 weeks old, body weight 275–300 g, Charles River Lab, MA) were used in this study. Rats were randomly divided into experimental (buckled) and control groups. All procedures were approved by the Institutional Animal Care and Use Committee of the University of Texas at San Antonio.

Animal preparation

Rats were anesthetized in a sealed chamber containing 5% isoflurane. Anesthesia was verified by the absence of reflex from a vigorous pinch to the rear footpad, and was maintained with 2% isoflurane through a cone-mask connected to a coaxial circuit. Enrofloxacin (10mg/kg, Sigma-Aldrich, St. Louis, MO) was administrated subcutaneously as a prophylaxis against post-operation sepsis. Glycopyrrolate (0.5 mg/kg, Sigma-Aldrich, St. Louis, MO) was administrated intramuscularly to protect the heart from vagal reflex and decrease bronchi secretions during operation. Heparin (0.7 mg/kg, Sigma-Aldrich, St. Louis, MO) was injected intraperitoneally to prevent thrombosis during vascular surgery. After anesthesia, rats were placed on a heating pad to maintain the body temperature at 37 °C. The hair in the neck region was clipped off, and the skin was prepared with a povidone-iodine scrub followed by 70% isopropyl alcohol. A sterile surgical drape was placed over the animal to isolate the surgical area.

Surgical procedure

A cervical midline incision (~ 2–3 cm long) was made along the neck to expose the carotid arteries. The left carotid artery was first exposed and dissected free from the surrounding tissues. Two suture markers (silk 11-0, Ningbo Medical Needle Co., China) were sewn onto the adventitia for length measurement. The artery was then ligated upstream and downstream of the markers, and the intervening segment (~6 – 10 mm) was excised to be used as the interposition graft (Fig 1). Next, the right carotid artery was exposed and 2

suture markers were sewn onto the adventitia. After clamping at both upstream and downstream, the vessel was cut off at the middle ("B" at the top panel of Fig. 1). The excised segment of left carotid artery was then grafted in between to reconnect the two separated ends by end-to-end anastomosis (6–8 interrupted sutures, silk 11-0, Fig. 1, bottom panel). The clamps were then released and the blood flow in the right carotid artery was restored. The implant increased the length of the vessel for the given distance between the aorta and the carotid bifurcation, and thus reduced the axial stretch ratio (and tension) in the vessel. The reduced stretch ratio decreased the critical buckling pressure of the vessel. As a result, the graft and right carotid artery buckled after the flow and pressure were restored (Fig 2, top-right panel). Finally, the wound was closed using nylon monofilament suture (4-0, Surgical Specialties Co., Reading, PA).

For rats in the control group, the procedures were repeated with the left carotid ligated and excised in the same way, but the right carotid was cut off and re-attached without interposition grafting.

After surgery, rats were closely monitored to ensure regular breathing, and the heating was continued until the rats were fully awake. Rats were then returned to the vivarium and maintained with regular food and water for up to 1 week.

The grafts and right carotid arteries were harvested 1 week after the surgery to examine geometric and structural changes. Twenty-four hours prior to harvesting, rats were treated with a single intraperitoneal injection of Bromodeoxyuridine (BrdU, 50mg/kg, Sigma-Aldrich, St. Louis, MO) to label new proliferating cells.[4] At harvesting, rats were anesthetized and prepared as described above. Grafts and right carotid arteries (Fig. 2 bottom-left panel) were exposed, photographed, and harvested. The grafts and right carotid arteries were photographed again after harvesting under load-free condition in PBS solution (Fig. 2 bottom-right panel), and then fixed with 2% paraformaldehyde (PFA, Sigma-Aldrich) overnight for H&E staining and immunohistochemistry. Wall remodeling was evaluated by examining the cell proliferation and MMP-2 and -9, which are families of enzymes known to break down the collagen matrix and are precursors of extracellular matrix remodeling.

Measurement of blood pressure and flow velocity

Rat blood pressure was measured via tail cuff using a MRBP system (IITC Life Science Inc., CA) pre-surgery, post-surgery, and on the day of harvesting (pre-harvesting). Blood flow in the right carotid artery was also measured using a Doppler system (Indus Instruments, TX) presurgery, post-surgery, and pre-harvesting.

Measurement of axial strain and tortuosity index

The grafts and right carotid arteries with suture markers were photographed at various time points during the surgery: a) before excision from the left carotid artery (baseline), b) after excision and set free in PBS at room temperature (day 0, load-free), c) immediately after grafted to the right carotid artery and blood flow was restored (day 0, under flow), d) seven days after grafting and right before harvesting (day 7, under flow), and e) after excision from the right carotid artery and set free in PBS at room temperature (day 7, load-free) (see Fig.

2). Vessel lengths and shapes between suture markers “A” on the grafts (Fig. 2) were measured off-line using ImagePro (MediaCybernetics, MD) to calculate axial strain, which was determined by

$$\varepsilon=(L_A - L_0)/L_0\times 100\% \quad (1)$$

where L_A is the vessel length between markers “A” at various time points, and L_0 is the vessel length between markers “A” after the vessel is excised and at load-free condition in PBS.

The tortuosity index (TI) was determined by

$$TI=L/D \quad (2)$$

where L and D are the curve length and straight distance between two ends of the graft, respectively.

Measurement of vessel diameter and thickness

Ring segments were cut off from the middle of buckled grafts, where the maximum deflection occurred, for fixation and histology. The circumferential lengths of the lumen (C_{lumen}) and outer (C_{out}) edges of the arterial wall were measured using ImagePro. The wall thickness was calculated as $t = (C_{out} - C_{lumen})/2\pi$, and the ratio of graft wall thickness to lumen diameter was determined by $(\pi t/ C_{lumen}) \times 100\%$.

BrdU staining

Cell proliferation was measured following a protocol used in our lab.[12, 28] Briefly, slides (5 μm in thickness) were deparaffinized and boiled with 10 mM sodium citrate buffer (Thermos Fisher Scientific Inc, NJ). Then the slides were permeabilized with 0.5% Triton X-100 (Sigma-Aldrich), blocked with 10% FCS-PBS, and incubated at room temperature for 30–60 min. Next, an anti-rat antibody (Roche Diagnostics GmbH, Germany) against BrdU was added 1:15 with 10% FCS-PBS, incubated at 37°C for 1 hour, and washed with PBS. Then a second antibody against mouse was added 1:20 with 1% FCS-PBS, incubated at 37°C for 1 hour, and washed with PBS. Slides were counterstained with Hoechst 33258 (Sigma-Aldrich, St. Louis, MO) at a concentration of 1 μg/ml at 37°C for 30 min.

Cell proliferation was examined and measured using fluorescent microscopy. The anti-BrdU positive cells and counterstained cells were counted in 5 view fields for each sample using ImagePro. Cell proliferation rate in each view field was calculated as the percentage of the number of BrdU positive cells over the total number of cells. The cell proliferation rate for each specimen was the average of the 5 view fields. To distinguish the outer and inner curves of buckled arteries, a longitudinal incision was made on the surface of the outer side of the curve before harvesting the segments. The incision became an opening slit on the cross sections of the BrdU stained slides.

Immunohistochemistry for MMP-2 and MMP-9

The procedure for MMP-2 staining was similar as that for BrdU staining, except that the first antibody added was mouse anti-MMP-2 and the second antibody was Cy3-conjugated goat antimouse (Jackson ImmuoResearch Lab, PA). Similarly, 5 view fields of each slide were photographed and all pictures were taken with the same exposure time of 5.31 s. The Integrated Optical Density (IOD) of MMP-2 expression was analyzed using ImagePro. In each view field, the area containing vessel tissues was selected and the IOD was measured and normalized by the tissue area (in pixel). This normalized IOD/pixel was then averaged for the 5 view fields.

The procedure for MMP-9 analysis was similar as that of MMP-2 except the first antibody added was rabbit anti-MMP-9 and the second antibody was Cy3-conjugated donkey anti-rabbit (Jackson ImmuoResearch Lab, PA).

Determination of arterial mechanical properties

Pressurized inflation tests were performed to measure the mechanical properties of the artery.[28] Briefly, one end of the artery was mounted to a cannula that was connected to a pressure meter and a syringe pump; the other end was tied to a luer stopper that moves freely with the end of the vessel. Arterial lumen pressure was gradually increased and recorded simultaneously with images of the deformed vessel. The vessel outer diameter and length were later measured along with the pressure.[28] The arterial wall was modeled as nonlinear anisotropic material with Fung's exponential strain energy function[8, 15]

$$w=\frac{1}{2}b_0e^{\mathrm{Q}},\ Q=b_1{E_\theta}^2+b_2{E_\mathrm{z}}^2+b_3{E_\mathrm{r}}^2+2b_4E_\theta E_\mathrm{z}+2b_5E_\mathrm{z}E_\mathrm{r}+2b_6E_rE_\theta \quad (3)$$

where b_0 and $b_1 - b_6$ are material constants and E_θ, E_z, E_r are the circumferential, axial, and radial strain components. Based on wall incompressibility and the equilibrium equation of a cylindrical artery under lumen pressure and axial tension, the lumen pressure and axial force are given by[14]

$$p=\int_{ri}^{re}[(1+2E_\theta)\frac{\partial w}{\partial E_\theta}-(1+2E_r)\frac{\partial w}{\partial E_r}]\frac{\mathrm{dr}}{r} \quad (4)$$

$$N=\pi\int_{ri}^{re}[2(1+2E_z)\frac{\partial w}{\partial E_z}-(1+2E_\theta)\frac{\partial w}{\partial E_\theta}-(1+2E_r)\frac{\partial w}{\partial E_r})]rdr+\pi r_i^2p \quad (5)$$

where r_i and r_e are the lumen and outer radii of the artery. By fitting equations (4) and (5) with experimental data, the material constants b_0 and $b_1 - b_6$ were determined using Matlab code.[28]

Computational buckling simulation

To estimate the changes of wall stress in buckled arteries, we simulated the buckling process of arteries using finite element analysis as previously described.[5] Briefly, static general analysis was performed to determine the critical buckling pressures and post-buckling wall stresses at given stretch ratios and in vivo pressures using commercial software package

Abaqus 6.11. Artery models were generated and meshed in Abaqus using quadratic hex elements. A small initial bend of ~0.1–0.2° along the central axis of the artery was given as small imperfection to facilitate buckling. The lumen pressure was gradually increased up to 100 mmHg for the grafts and 200mmHg for the baseline (to exceed the critical pressures), respectively. The computational model was first validated for the case of straight cylindrical vessels by comparing the model results with analytical solutions.

The initial free length and outer diameter, the length post-grafting (hence the stretch ratio), and the *in vivo* systolic pressure of the left carotid artery grafts measured from the experiments were used in the simulations for each artery. The boundary conditions at both ends of the grafts were assumed to be restrained from rotation but free to radial dilation. The material properties of Fung energy function obtained from inflation tests described above were used for the simulations. For comparison, simulations were also performed for each graft before excised from the left carotid, where the graft was under normal in vivo strain (stretch ratio).

Statistical analysis

All values were expressed by Mean ± SD. Statistical significance was determined with $p < 0.05$ using a 2-way ANOVA followed by a Tukey's post hoc analysis (JMP, SAS Institute Inc.).

Results

Left-to-right carotid artery grafting was successfully implemented in 5 rats. All grafts buckled when the blood flow was restored after anastomosis. The grafts remained patent until harvesting.

Blood flow and axial strain

There was no significant change of blood pressure or blood flow velocity among pre-surgery, post-surgery, and 1 week after surgery in either the buckled group or the control group ($p > 0.05$).

The axial strain in the grafts decreased significantly from the initial value (baseline) of 41±12% to 3±8% post-grafting (n=5, $p < 0.05$, Fig. 3). It then increased to 13±8% in 1 week, but the increase was statistically insignificant.

Tortuosity index

The carotid grafting yielded buckling and increased the tortuosity of the grafts (Fig. 4). At baseline (before excision from the left carotid artery) the carotid arteries were nearly straight such that the in situ TI ≈ 1. Immediately after surgery (at day 0 under flow), TI in the buckled group significantly increased to 1.22±0.15 (n=5, $p = 0.03$). It further increased to 1.28±0.34 one week later (day 7), but this increase was insignificant ($p = 0.56$) compared with day 0.

At load-free conditions, the tortuosity index TI of the grafts at day 0 and day 7 showed no statistical difference (1.05±0.03 vs. 1.08±0.02, $p = 0.09$), indicating no significant change in the natural shape of the grafts.

In the control group, the right carotid arteries under flow in vivo remained straight before and after the mock surgery as well as at day 7 post-surgery. TI at day 7 was 1.01±0.004 (n=3) under flow and 1.04±0.01 (n=3) after excision at load-free condition, showing no statistical difference.

Cell proliferation

Compared with the control group, the cell proliferation in the buckled group increased remarkably at 1 week (13.2±6.8% vs. 2.43±2.3% in control group) ($p < 0.001$) (Fig. 5). But there was no significant difference in cell proliferation between the inner side (14.6±7.7%) and outer side (13.3±4.0%) ($p > 0.05$) of curved grafts.

MMP-2 and MMP-9

Compared with the control group, the expression of MMP-2 in the buckled group increased significantly by 4.2-fold at 1 week ($p < 0.001$), but the expression of MMP-9 did not increase significantly ($p = 0.63$) (Fig. 6).

Ratio of wall thickness to lumen diameter

The ratio of arterial wall thickness to lumen diameter (Fig. 7) in the buckled group had no statistical difference ($p = 0.61$) compared with the control group, suggesting no wall thickening in the buckled arteries after surgery. No intimal hyperplasia was observed from histology slides either.

Computational simulation results

The pressurized inflation test was done for one carotid artery graft. The values of the material constants b_0 and b_1 to b_6 determined were 100.0kPa, 0.686, 0.498, 0.749, 0.040, 0.001, and 0.001, respectively. Using these material constants, the buckling process was simulated for each graft with its specific dimensions (outer diameter and length) and loads (pressure and axial stretch ratio). A wall thickness to outer diameter ratio of 0.1 (measured from one artery) was used for all simulations due to lack of wall thickness data of individual grafts.

Simulation results demonstrated that the critical buckling pressure was significantly lower in the grafts post-surgery compared to their baseline before excision (35.6 ± 7.7 mmHg vs. 125.7 ± 43.8 mmHg, p< 0.01, Fig. 8a). Thus, under in vivo lumen pressure (~ 100 mmHg), carotid arteries at normal in vivo axial strain initially did not buckle (even without considering surrounding tissue support), but buckled as grafts with reduced axial strain post-surgery. The average tortuosity index TI post-grafting determined from the simulations was comparable to the experimental measurement (1.19 ± 0.04 vs. 1.22 ± 0.15, p=0.75, Fig. 8b). Figure 8(c) compares the mid-wall stresses in arteries post-grafting (buckled) and at the baseline (un-buckled). The mid-wall stress indicated the mean stress across the wall thickness. Wall stresses were axisymmetric in un-buckled arteries at baseline (under normal

in vivo axial strain pre-excision). However, in buckled arteries under the same normal pressure, there were significant decreases in circumferential and axial stresses on the inner side of the curve ($p<0.01$) and a significant increase in axial stress on the outer curve side ($p=0.02$), though no significant change in circumferential stress on the outer curve side (Fig. 8c). The wall stresses at both the lumen and outer wall demonstrated similar trends. Note that axial strains were 41% and 3% respectively pre-excision and post-grafting.

Discussion

In this study, we successfully developed a carotid artery buckling model in rats and determined the early stage of wall remodeling in buckled arteries. Our results showed that buckled arteries demonstrated a significantly higher cell proliferation and MMP-2 expression 1 week post-surgery. Artery tortuosity index also increased though the increase was statistically insignificant. In addition, artery (graft) tortuosity index at the load-free condition at day 0 and day 7 showed no significant difference, suggesting no permanent shape change in artery geometry 1 week post-surgery.

The artery buckling model was designed based on our previous work which demonstrated that reducing axial strain would reduce the critical buckling pressure.[13, 16] By using interpositional grafting of rat carotid arteries, the axial strain in the grafts significantly decreased from its baseline value of 41% to 3% and we were able to generate artery buckling at normal physiological pressure and flow conditions, without causing hypertensive or hyper-flow condition. Our data confirmed that there was no significant change in blood pressure or flow rate in the carotid before and after grafting. This feature allowed us to specify the observed changes to strain reduction-induced buckling, without the effects of pressure and flow rate. Note that artery buckling under the lumen pressure became inevitable at the low axial strain level used in this work. While additional studies in our lab have shown that the reduction of axial stretch and buckling can be separated in vitro at a higher axial strain,[37] the low axial strain-induced buckling is more clinically relevant since many tortuous arteries observed in human, such as in aged populations, are associated with low axial strain.[6, 11, 32]

Previously, Jackson and colleagues[24] reduced the axial strain in rabbit carotid artery from 62% to 33%, and found that the reduction of axial tension led to tortuous arteries *in vivo* 5 weeks post-surgery. However, they were not intending to create buckling and did not report seeing tortuous shape immediately after grafting. It is not clear whether the reduction of axial strain to 33% was enough to generate artery buckling. In addition, since artery tortuosity was observed from vascular casting obtained under *in vivo* pressure, it was unclear whether the arteries would stay tortuous if excised and set free. In the current study, we have observed that arteries were tortuous under flow but would restore to their initial shapes at load-free condition at day 7. This observation suggests that artery tortuosity is reversible at an early stage. Buckled arteries may take a much longer time to adapt and become permanently tortuous.

We used TI defined in Eq. (2) to describe the level of vessel tortuosity. There have been reports of other indices used.[17] We also calculated the TI as given by the ratio of maximum

deflection (δ) to distance (D), δ/D, and the summation of squared ratios of all chords ($8/3 \times \Sigma_k(\delta_k / D_k)$).[17, 18] The results showed similar tends as given in Fig. 4 without statistical difference among all groups.

Our simulation showed significant decreases of circumferential and axial stresses at the inner curve of buckled artery, and significant increase of axial stress at the outer curve (Fig. 8c). These changes in wall stresses resulted from the reduction in axial strain and the bending deformation (buckling). While the reduction in axial strain decreased the axial stress globally, the bending increased the axial stress at the outer curve and further reduced the axial stress at the inner curve. Due to the coupling between axial and circumferential stresses and strains as seen in the strain energy function (Eq. 3), the reduction in axial strain also decreased the circumferential stress globally. The vessel length per se did not affect the stresses in the vessel wall since theoretical and computational simulations showed that stresses in cylindrical vessels are determined by lumen pressure and axial strain but independent of the vessel length. However, the added length of the graft significantly reduced the axial strain to 3%. At this low axial strain, the artery buckling became inevitable under the lumen pressure. Buckling attenuated axial strain reduction on the outer curve side but enhanced the reduction on the inner curve side, and thus led to stress differences between the inner and outer curve sides of the arterial wall. These trends in stresses were consistent with theoretical analysis for small deflection at critical pressure.[14]

MMP-2 and MMP-9 are two primary matrix metalloproteinases that breakdown extracellular matrix in artery remodeling.[9] Both MMP-2 and -9 activities are significantly upregulated in cases such as injury-induced remodeling and contribute to smooth muscle cells migration.[10] Knockout of MMP-2 or MMP-9 both decreased smooth muscle cells migration and intimal hyperplasia in the carotid ligation model in mice.[26, 27] Differences between MMP-2 and 9 are also seen in other cases. For example, MMP-2 is produced and detectable in media and its expression is upregulated by shear stress increase in arteries;[35] whereas MMP-9 expressed primarily by inflammatory cells and its expression is undetectable in uninjured vessels.[10] MMP-9 but not MMP-2 is essential for collagen organization.[26] MMP-9 expression significantly increased along with outward arterial remodeling.[10] In the present study, MMP-2 expression and cell proliferation increased remarkably 1 week post-surgery in buckled arteries but MMP-9 expression was not changed. This was most likely due to the changes of wall stress and shear stress induced by arterial buckling shape.[17] Altering the flow shear stress and wall stress in the arterial wall are well known to stimulate vascular cell functions, including cell proliferation and apoptosis.[12, 21, 34, 36] Our simulation demonstrated significant changes in wall stresses in buckled arteries post-grafting, especially in axial stress (Fig. 8c). On the other hand, extreme care was given in the surgical process to minimize vessel injury. Cell proliferation and MMPs measurements were made on tissue samples cut far away from the anastomosis sites. In addition, there was no upregulation of MMP-9 expression which indicated little injury or inflammatory response in the vessels. Therefore, the observed changes in cell proliferation and MMP-2 were most likely resulted from the stress changes in buckled arteries (due to the low axial strain–induced buckling).

Furthermore, cell proliferation and MMP expression observed in the present study were similar to the reported changes in rabbit carotid arteries due to elevated or reduced axial tension[23, 24] and in porcine arteries under altered pressure pulsatility.[19] The increases of cell proliferation and MMP-2 expression were also consistent with the results of in vitro buckling study of porcine carotid arteries in organ culture.[37, 38]

The limitations of this study include the small sample size and the short duration of the observation due to budget and resource constraints. The short-term design was aimed to quickly validate the model within limited time and resources. In addition, the mechanical properties of the buckled grafts were not examined for concerning the stiffness changes would be minimal due to the short experiment duration. Another reason was to avoid using the grafts for other tests prior to grafting to preserve the vascular function and to achieve maximal length of the grafts for this initial study. The mechanical tests need to be done in future studies to evaluate the possible changes in wall remodeling for long-term studies. Though limitations exist, our study has achieved the goal of establishing a new animal model of artery buckling and demonstrated the feasibility of applying this model for studying wall remodeling in artery buckling. Future studies will examine the long-term adaptation of buckled arteries. In addition, the model could be potentially modified into a vein grafting model[30] to study the remodeling of buckled veins.

In conclusion, rat left-to-right carotid artery grafting is a good animal model for studying wall remodeling in buckled arteries. Artery buckling alters the wall stress and stimulates cell proliferation and matrix remodeling. This study set a basis for further studies to elucidate the mechanisms and processes of the development of tortuous arteries.

Acknowledgments

This work was supported by internal funds from UTSA. It was also partially supported by CAREER award #0644646 from the National Science Foundation and grant R01HL095852 from the National Institute of Health. We thank Dr. Shu Q Liu of Northwestern University for his helpful suggestions. We also thank Dr. Yangming Xiao in our lab and staff in the Laboratory Animal Resources Center of UTSA, and Dr. Merry Lindsey's lab for their kind help.

References

1. Aleksic M, Schutz G, Gerth S, Mulch J. Surgical approach to kinking and coiling of the internal carotid artery. J Cardiovasc Surg (Torino). 2004; 45(1):43–48.
2. Brown WR, Moody DM, Challa VR, Thore CR, Anstrom JA. Venous collagenosis and arteriolar tortuosity in leukoaraiosis. J Neurol Sci. 2002; 203–204:159–163.
3. Cheung AT, Ramanujam S, Greer DA, Kumagai LF, Aoki TT. Microvascular abnormalities in the bulbar conjunctiva of patients with type 2 diabetes mellitus. Endocr Pract. 2001; 7(5):358–363. [PubMed: 11585371]
4. Cho YK, Farbman AI, Smith DV. The timing of alpha-gustducin expression during cell renewal in rat vallate taste buds. Chem Senses. 1998; 23(6):735–742. [PubMed: 9915120]
5. Datir P, Lee AY, Lamm SD, Han HC. Effects of Geometric Variations on the Buckling of Arteries. Int J Appl Mech. 2011; 3(2):385–406. [PubMed: 22287983]
6. Del Corso L, Moruzzo D, Conte B, Agelli M, Romanelli AM, Pastine F, Protti M, Pentimone F, Baggiani G. Tortuosity, kinking, and coiling of the carotid artery: expression of atherosclerosis or aging? Angiology. 1998; 49(5):361–371. [PubMed: 9591528]

7. Fung, YC. Biomechanics : motion, flow, stress, and growth. New York: Springer-Verlag; 1990. p. 569xv
8. Fung, YC. Biomechanics: Mechanical Properties of Living Tissues. 2nd ed. ed.. New York: Springer Verlag; 1993.
9. Galis ZS, Khatri JJ. Matrix metalloproteinases in vascular remodeling and atherogenesis: the good, the bad, and the ugly. Circ Res. 2002; 90(3):251–262. [PubMed: 11861412]
10. Godin D, Ivan E, Johnson C, Magid R, Galis ZS. Remodeling of carotid artery is associated with increased expression of matrix metalloproteinases in mouse blood flow cessation model. Circulation. 2000; 102(23):2861–2866. [PubMed: 11104745]
11. Han HC, Ku DN, Vito RP. Arterial wall adaptation under elevated longitudinal stretch in organ culture. Annals of Biomedical Engineering. 2003; 31(4):403–411. [PubMed: 12723681]
12. Han HC, Ku DN, Vito RP. Arterial wall adaptation under elevated longitudinal stretch in organ culture. Ann Biomed Eng. 2003; 31(4):403–411. [PubMed: 12723681]
13. Han HC. A biomechanical model of artery buckling. J Biomech. 2007; 40(16):3672–3678. [PubMed: 17689541]
14. Han HC. Nonlinear buckling of blood vessels: a theoretical study. J Biomech. 2008; 41(12):2708–2713. [PubMed: 18653191]
15. Han HC. Blood vessel buckling within soft surrounding tissue generates tortuosity. J Biomech. 2009; 42(16):2797–2801. [PubMed: 19758591]
16. Han HC. The theoretical foundation for artery buckling under internal pressure. J Biomech Eng. 2009; 131(12):124501. [PubMed: 20524735]
17. Han HC. Twisted blood vessels: symptoms, etiology and biomechanical mechanisms. J Vasc Res. 2012; 49(3):185–197. [PubMed: 22433458]
18. Hart WE, Goldbaum M, Cote B, Kube P, Nelson MR. Measurement and classification of retinal vascular tortuosity. Int J Med Inform. 1999; 53(2–3):239–252. [PubMed: 10193892]
19. Hayman DM, Zhang JZ, Liu Q, Xiao YM, Han HC. Smooth muscle cell contraction increases the critical buckling pressure of arteries. Journal of Biomechanics. 2013; 46(4):841–844. [PubMed: 23261241]
20. Hiroki M, Miyashita K, Oda M. Tortuosity of the white matter medullary arterioles is related to the severity of hypertension. Cerebrovasc Dis. 2002; 13(4):242–250. [PubMed: 12011548]
21. Hsu S, Chu JS, Chen FF, Wang A, Li S. Effects of Fluid Shear Stress on a Distinct Population of Vascular Smooth Muscle Cells. Cell Mol Bioeng. 2011; 4(4):627–636. [PubMed: 22924082]
22. Humphrey, JD. Cardiovascular solid mechanics : cells, tissues, and organs. New York: Springer; 2002. p. 757xvi
23. Jackson ZS, Gotlieb AI, Langille BL. Wall tissue remodeling regulates longitudinal tension in arteries. Circulation Research. 2002; 90(8):918–925. [PubMed: 11988494]
24. Jackson ZS, Dajnowiec D, Gotlieb AI, Langille BL. Partial off-loading of longitudinal tension induces arterial tortuosity. Arterioscler Thromb Vasc Biol. 2005; 25(5):957–962. [PubMed: 15746437]
25. Jakob M, Spasojevic D, Krogmann ON, Wiher H, Hug R, Hess OM. Tortuosity of coronary arteries in chronic pressure and volume overload. Cathet Cardiovasc Diagn. 1996; 38(1):25–31. [PubMed: 8722854]
26. Johnson C, Galis ZS. Matrix metalloproteinase-2 and -9 differentially regulate smooth muscle cell migration and cell-mediated collagen organization. Arterioscler Thromb Vasc Biol. 2004; 24(1): 54–60. [PubMed: 14551157]
27. Kuzuya M, Kanda S, Sasaki T, Tamaya-Mori N, Cheng XW, Itoh T, Itohara S, Iguchi A. Deficiency of gelatinase a suppresses smooth muscle cell invasion and development of experimental intimal hyperplasia. Circulation. 2003; 108(11):1375–1381. [PubMed: 12939223]
28. Lee AY, Han B, Lamm SD, Fierro CA, Han HC. Effects of elastin degradation and surrounding matrix support on artery stability. Am J Physiol Heart Circ Physiol. 2012; 302(4):H873–H884. [PubMed: 22159998]
29. Liu Q, Han HC. Mechanical buckling of arterioles in collateral development. J Theor Biol. 2013; 316:42–48. [PubMed: 23034307]

30. Liu SQ. Influence of tensile strain on smooth muscle cell orientation in rat blood vessels. J Biomech Eng. 1998; 120(3):313–320. [PubMed: 10412397]

31. Metz H, Murray-Leslie RM, Bannister RG, Bull JW, Marshall J. Kinking of the internal carotid artery. Lancet. 1961; 1(7174):424–426. [PubMed: 13769898]

32. Nichols, WW.; O'Rourke, MF. McDonald's Blood Flow in Arteries: Theoretical, Experimental, and Clinical Principles. 4th Ed. ed.. London: Arnold Publisher; 2005. p. 67-94.

33. Owen CG, Newsom RS, Rudnicka AR, Barman SA, Woodward EG, Ellis TJ. Diabetes and the tortuosity of vessels of the bulbar conjunctiva. Ophthalmology. 2008; 115(6):e27–e32. [PubMed: 18423868]

34. Rennier K, Ji JY. Effect of shear stress and substrate on endothelial DAPK expression, caspase activity, and apoptosis. BMC Res Notes. 2013; 6:10. [PubMed: 23305096]

35. Sho E, Sho M, Singh TM, Nanjo H, Komatsu M, Xu C, Masuda H, Zarins CK. Arterial enlargement in response to high flow requires early expression of matrix metalloproteinases to degrade extracellular matrix. Exp Mol Pathol. 2002; 73(2):142–153. [PubMed: 12231217]

36. Wong LC, Langille BL. Developmental remodeling of the internal elastic lamina of rabbit arteries: effect of blood flow. Circ Res. 1996; 78(5):799–805. [PubMed: 8620599]

37. Xiao Y, Hayman D, Khalafvand SS, Lindsey ML, Han HC. Artery buckling stimulates cell proliferation through NF-κB signaling. Am J Physiol Heart Circ Physiol. 2014 (in revision).

38. Xiao YM, Chesnutt JK, Han HC. Artery buckling stimulates MMP-2 expression in arterial wall. BMES Annual Meeting, Sept. 25–28, Seattle, Washington. 2013

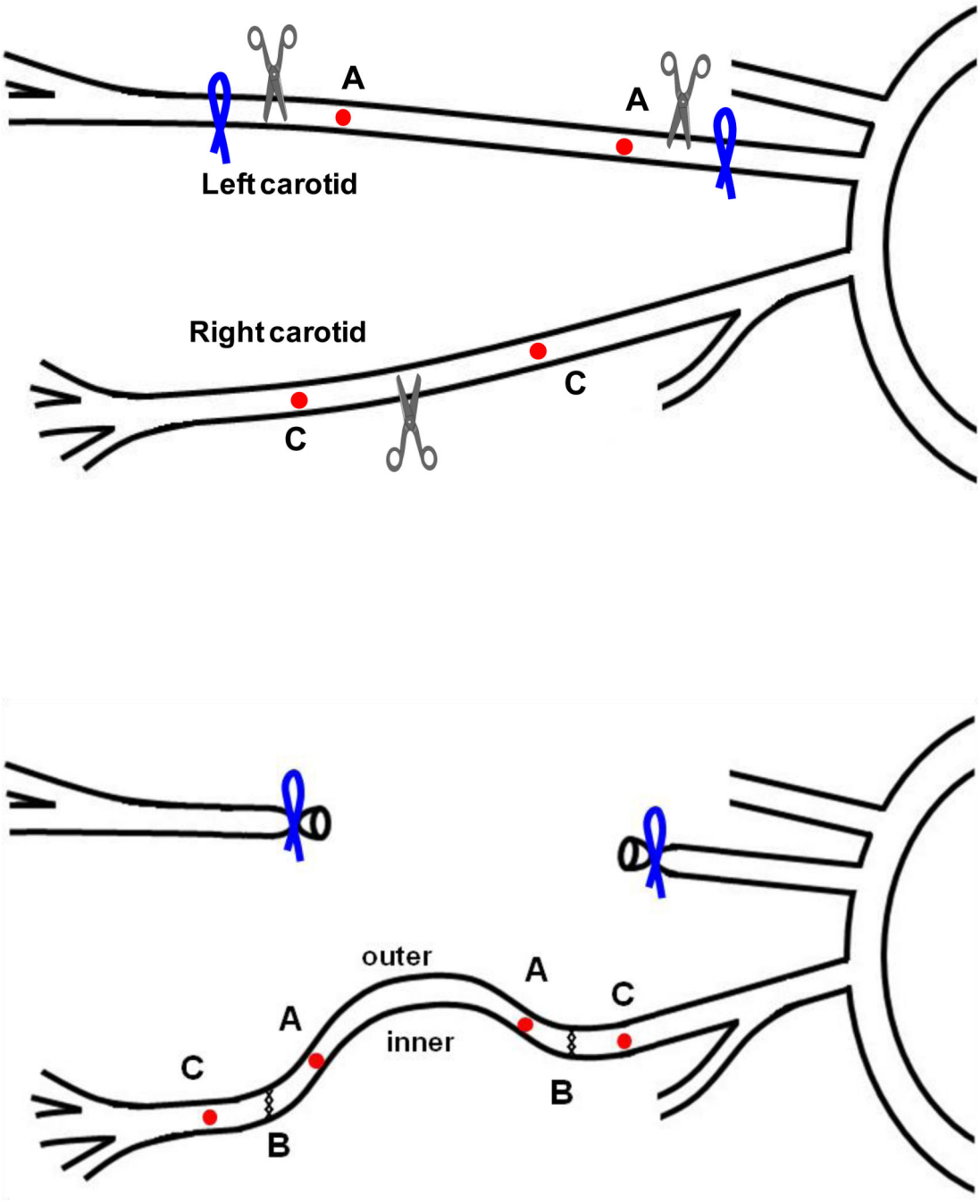

Figure 1.

Schematic illustration of the left-to-right carotid artery grafting. A segment of the left carotid artery is harvested and implanted into the right carotid artery via end-to end anastomosis. “A” & “C”, markers on the graft; “B”, cut off and anastomosis sites; “inner” and “outer” indicate the inner curve and outer curve sides of the curved vessel, respectively.

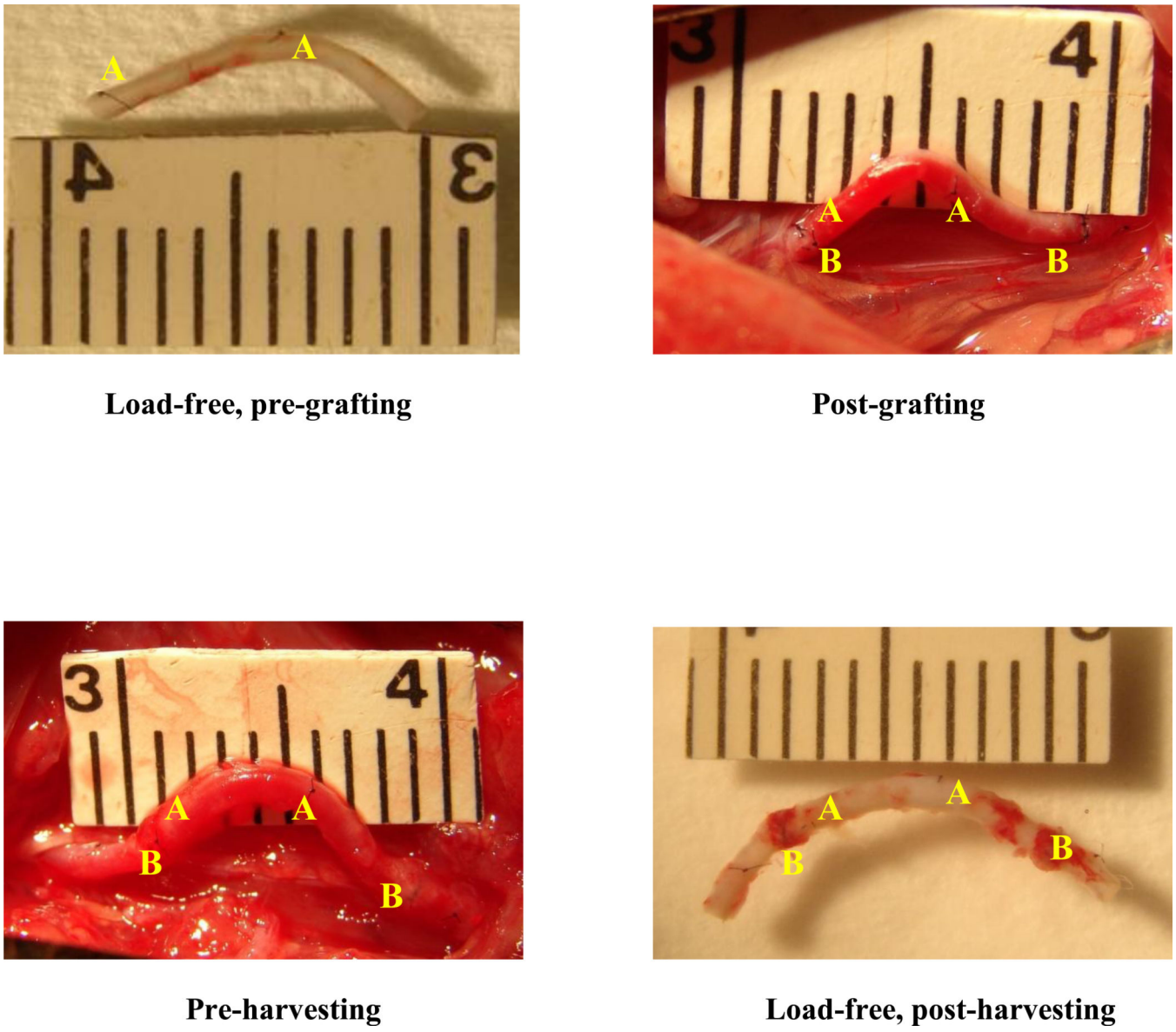

Figure 2.

Photographs of a typical left carotid artery segment at 4 stages of experiment/procedure. i) After excision and load-free in PBS (top left); ii) immediately post-grafting (top right); iii) pre-harvesting (bottom left); and iv) post-harvesting and load-free in PBS (bottom right). "A", markers on the graft; "B", anastomosis sites.

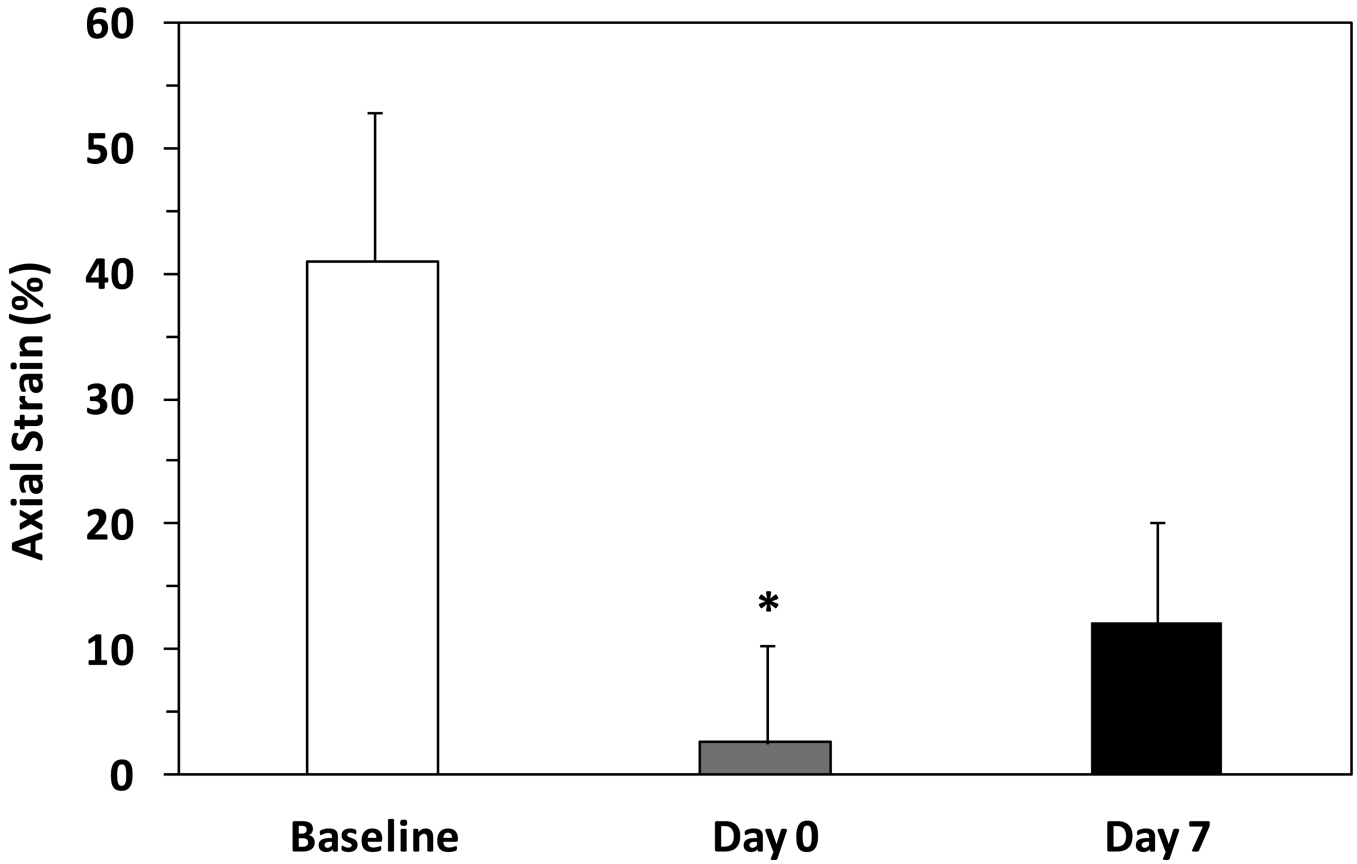

Figure 3.

Comparison of axial strain (mean ± SD, n=5) in carotid arteries at baseline, immediately post-grafting (Day 0), and 1 week after surgery (Day 7) in buckled shape. * $p < 0.05$ compared with baseline.

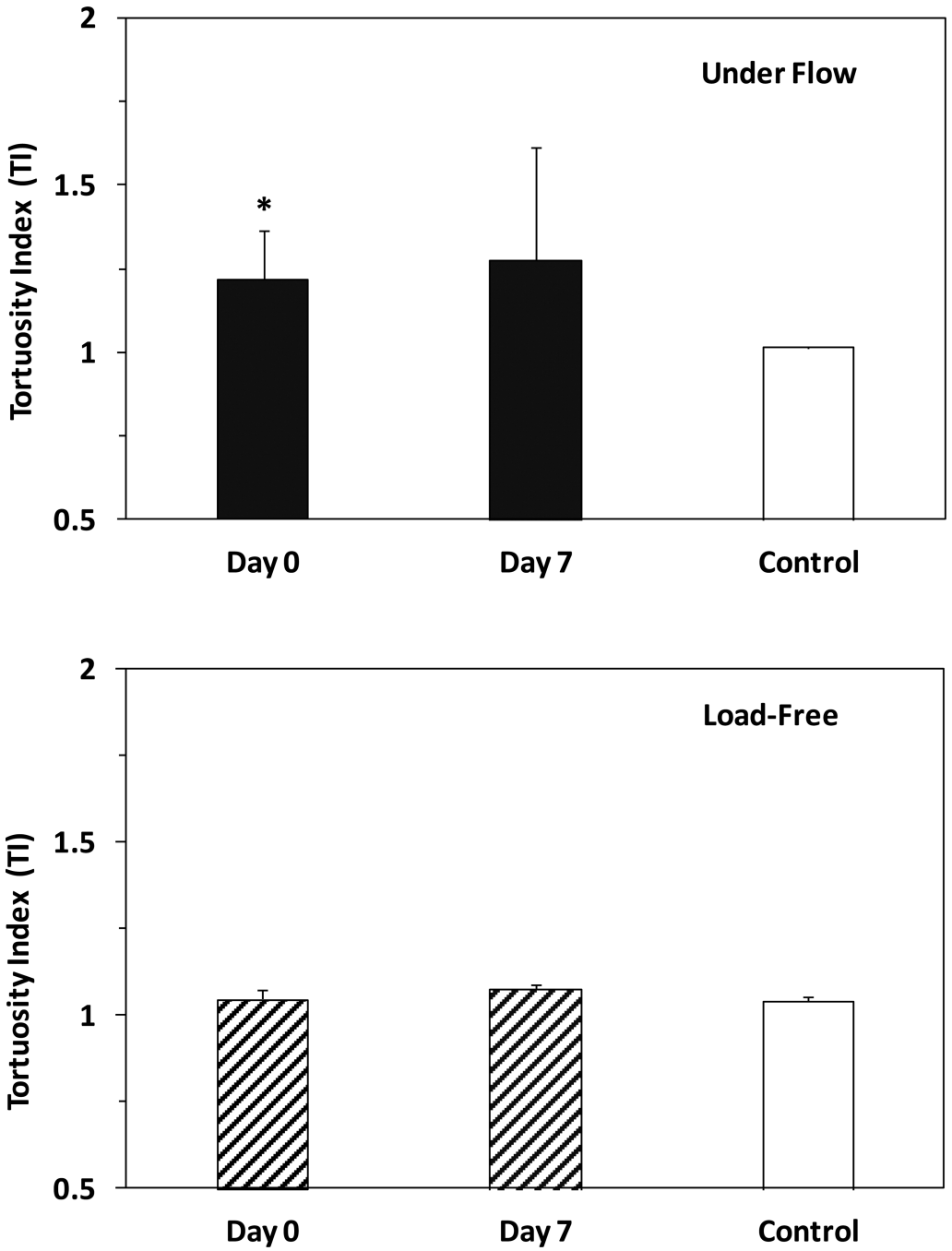

Figure 4.

Comparison of tortuosity index (TI, mean ± SD, n=5) in the buckled group and control group. Top: TI of grafts under flow in vivo. Bottom: TI of grafts load-free in PBS. * $p < 0.05$ compared with control.

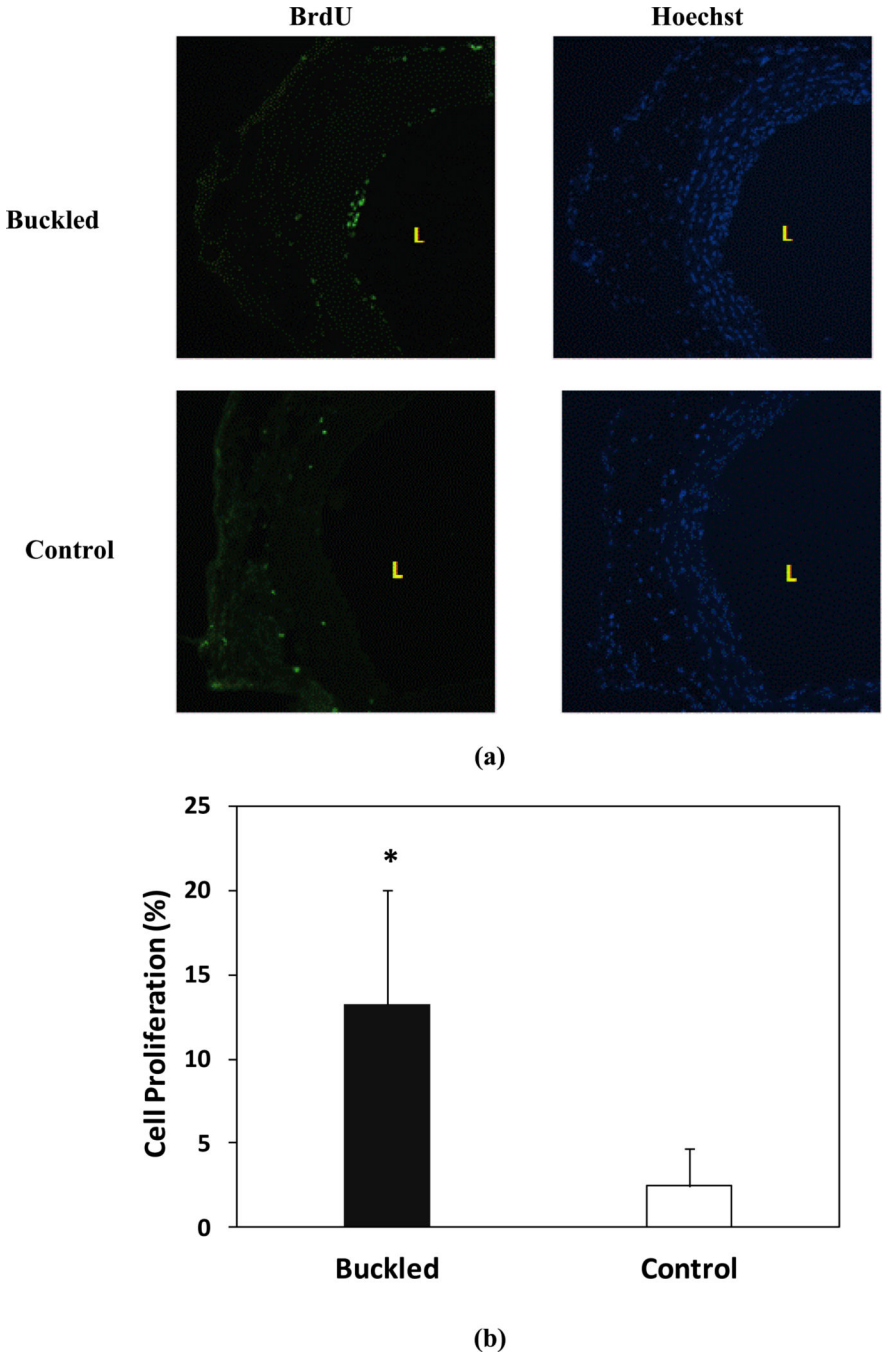

Figure 5.

Cell proliferation in buckled arteries. (a) Proliferative cells labeled by BrdU staining (green fluorescence, left panels) and all cell nuclei counterstained by Hoechst staining (blue fluorescence, right, panel). “L” indicates the lumen of the vessel. (b) Comparison of cell proliferation ratio (mean ± SD, n=5) in the buckled and control group. * $p < 0.05$ compared with control.

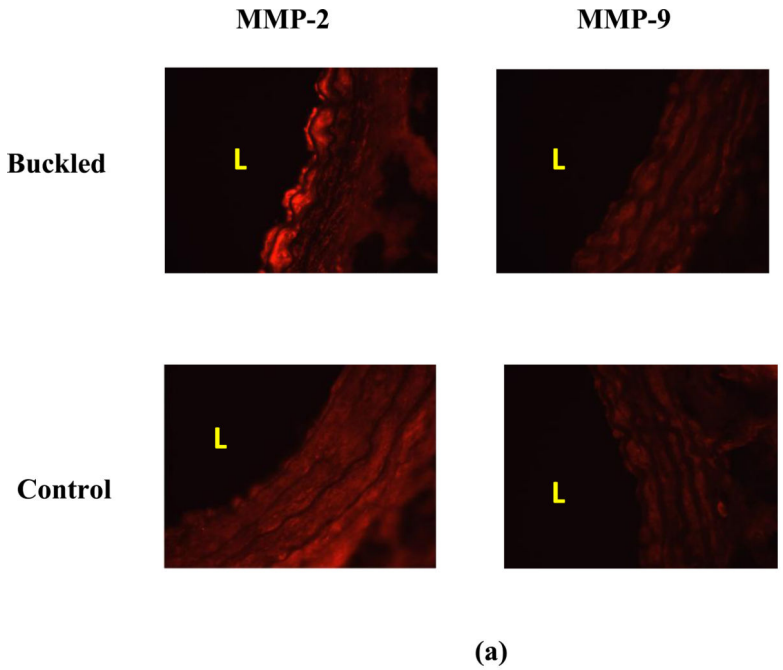

(a)

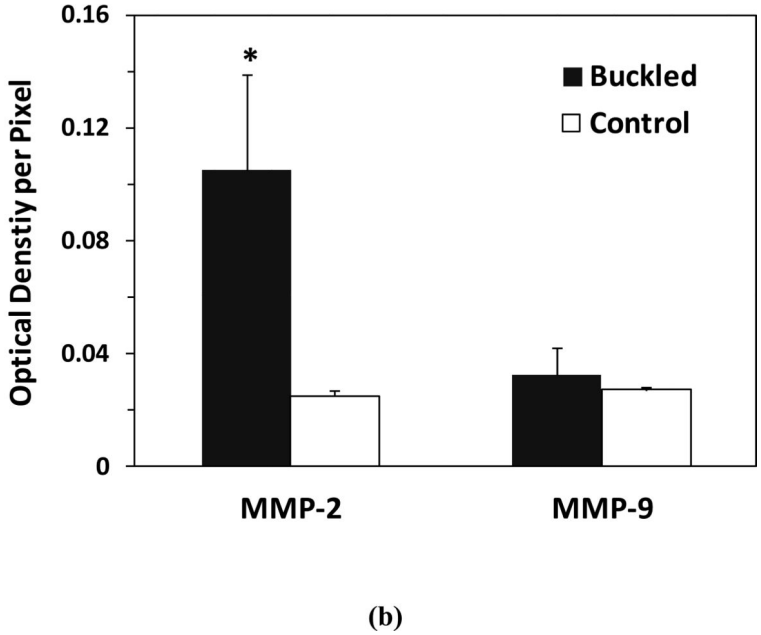

(b)

Figure 6.

Matrix metalloprotinaese-2 (MMP-2) and -9 (MMP-9) levels in buckled arteries. (a) Representative photographs of vessel cross-section demonstrating the expressions of MMP-2 and -9 in buckled grafts and control arteries. Light red indicates positive MMP expression “L” indicates the lumen of the vessel. (b) Comparison of MMP-2 and MMP-9 level measured by the integrated optical density per pixel in the buckled and control group (mean ± SD, n=5). * $p < 0.05$ compared with control.

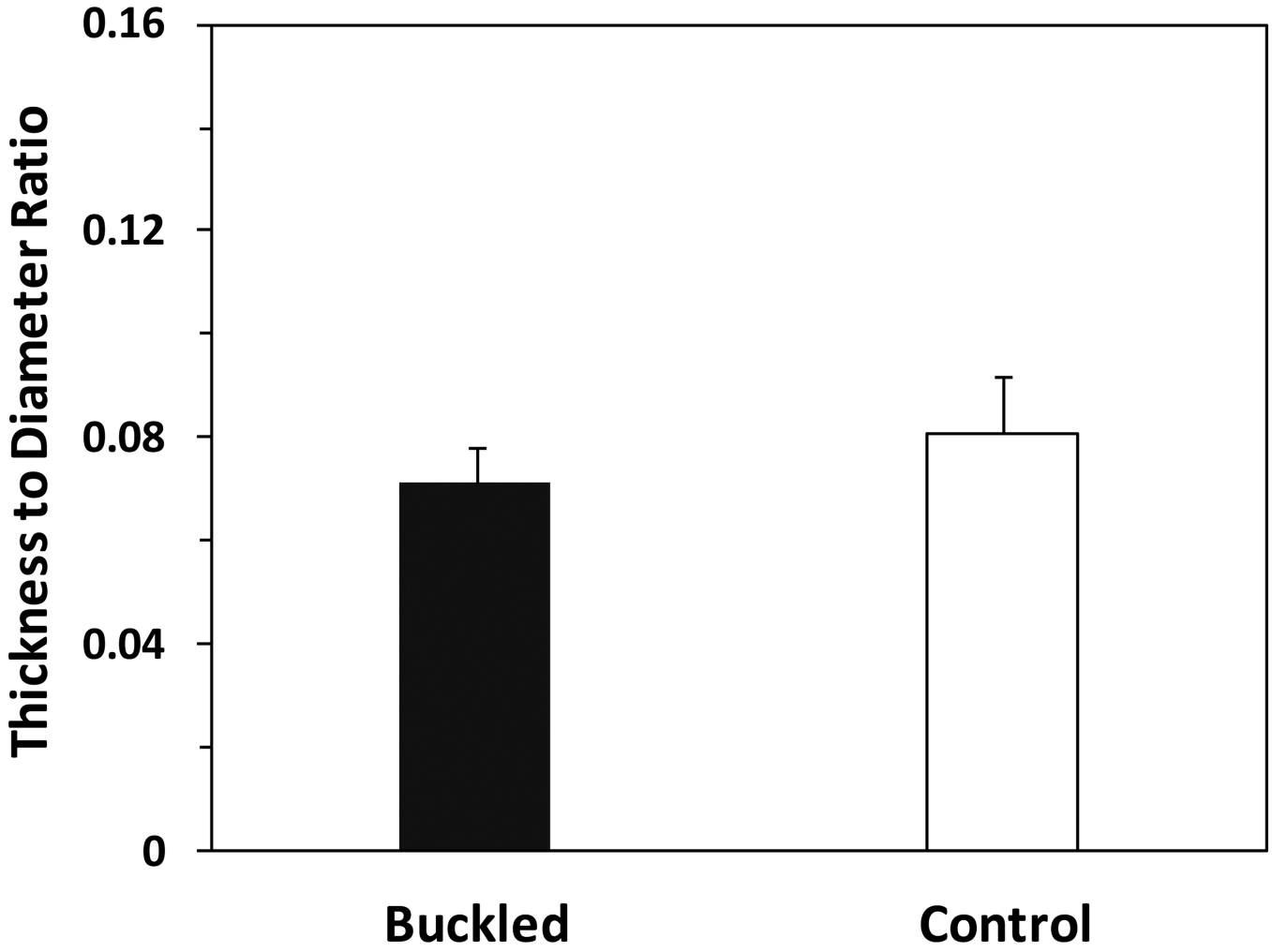

Figure 7.
Comparison of wall thickness to lumen diameter ratio in the buckled and control groups (mean ± SD, n=5).

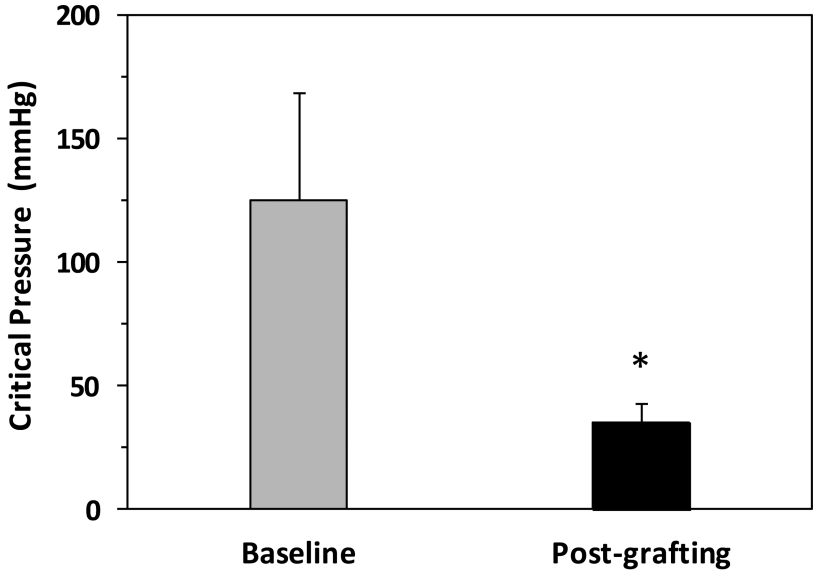

(a)

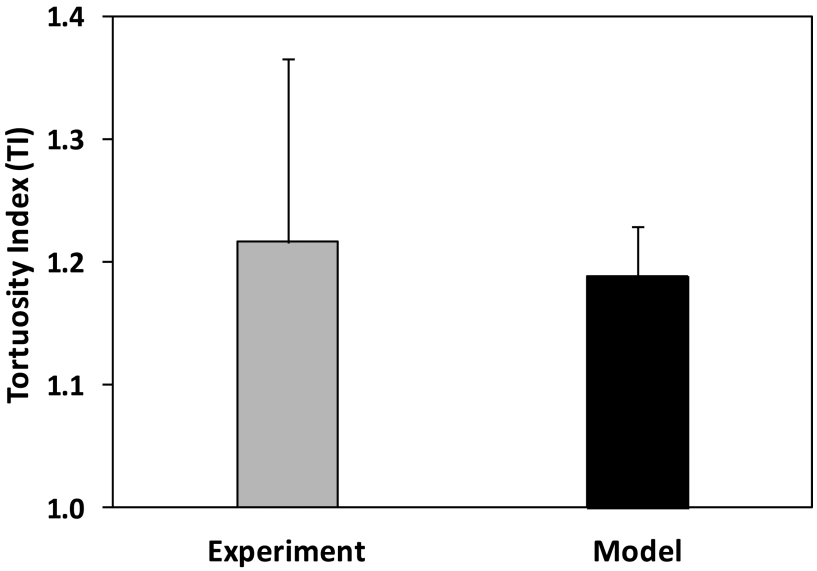

(b)

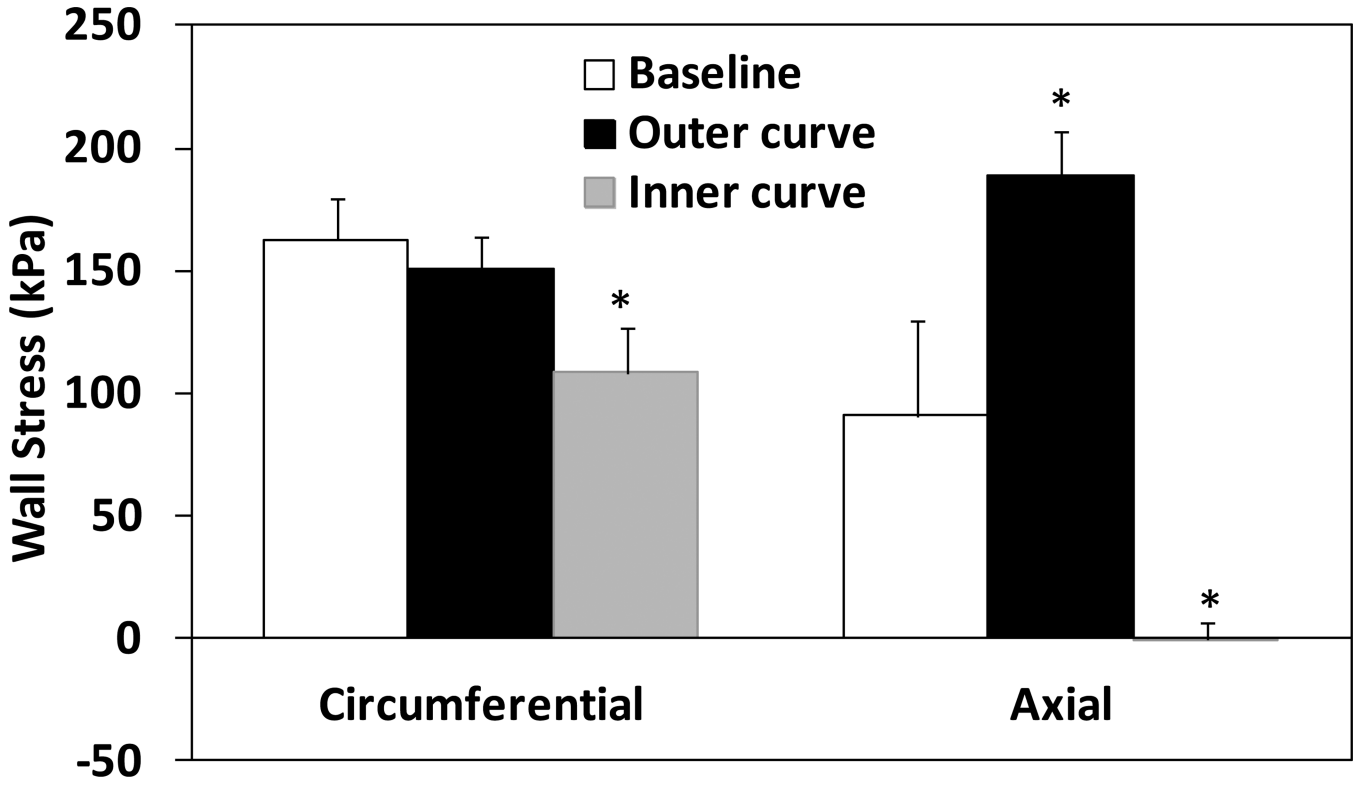

(c)

Figure 8.

Computational simulation results. (a) Comparison of critical buckling pressure of the left carotid artery segments at baseline (pre-excision) and post-grafting. (b) Comparison of tortuosity index TI determined from simulations and from experimental measurements. (c) Comparison of mid-wall stresses at the outer and inner curve sides in arteries post-grafting (buckled) and at baseline (straight). Arteries were under their in vivo lumen pressures. * $p < 0.05$ compared with baseline.